Langmuir

Article

pubs.acs.org/Langmuir

# Irreversible Adsorption-Driven Assembly of Nanoparticles at Fluid Interfaces Revealed by a Dynamic Surface Tension Probe

Navid Bizmark,[†] Marios A. Ioannidis,*[,†] and Dale E. Henneke[‡]

[†]Department of Chemical Engineering, University of Waterloo, 200 University Avenue West, Waterloo, Ontario N2L 3G1, Canada

[‡]Department of Materials Engineering, New Mexico Institute of Mining and Technology, 801 Leroy Place, Socorro, New Mexico 87801, United States

Supporting Information

**ABSTRACT:** Adsorption-driven self-assembly of nanoparticles at fluid interfaces is a promising bottom-up approach for the preparation of advanced functional materials and devices. Full realization of its potential requires quantitative understanding of the parameters controlling the self-assembly, the structure of nanoparticles at the interface, the barrier properties of the assembly, and the rate of particle attachment. We argue that models of dynamic surface or interfacial tension (DST) appropriate for molecular species break down when the adsorption energy greatly exceeds the mean energy of thermal fluctuations and validate alternative models extending the application of generalized random sequential adsorption theory to nanoparticle adsorption at fluid interfaces. Using a model colloidal system of hydrophobic, charge-stabilized ethyl cellulose nanoparticles at neutral pH, we demonstrate the potential of DST measurements to reveal information on the energy of adsorption, the adsorption rate constant, and the energy of particle−interface interaction at different degrees of nanoparticle coverage of the interface. These findings have significant implications for the quantitative description of nanoparticle adsorption at fluid interfaces.

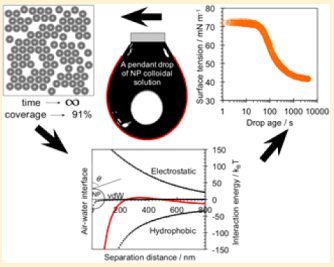


## INTRODUCTION

Like surfactants, solid particles can adsorb at gas−liquid and liquid−liquid interfaces. Thermodynamics favors the adsorption process, which results in the reduction of surface or interfacial tension. Thus, like surfactants, colloidal particles can act as emulsifiers, stabilizing so-called "Pickering" emulsions.[1,2] The following equation relates the reduction of surface energy ($\Delta E$) associated with the adsorption of a single spherical particle to its radius ($r$) and wettability[3−5]

$$\Delta E = -\gamma_0 \pi r^2 (1 - |\cos\theta|)^2 \quad (1)$$

where $\gamma_0$ denotes the surface (interfacial) tension of the pristine interface and $\theta$ is the contact angle of a single particle at the interface measured through the aqueous phase. Unlike surfactants, however, the adsorption energy of particles can exceed the mean energy of thermal fluctuations by several orders of magnitude ($|\Delta E| \gg k_B T$), meaning that colloidal particle adsorption at fluid interfaces is effectively irreversible.[3,6,7] As a result of much stronger attachment to the interface, solid particles inhibit bubble/drop coalescence and coarsening more effectively than surfactants,[8] resulting in foams and emulsions of exceptional stability.[3,9−12] In the past decade, numerous products and processes involving nanoparticle-stabilized foams and emulsions have been investigated in a variety of fields ranging from materials science[12] to catalysis,[13] and from food science[6] to biomedicine[11] and sensing.[14,15] In addition to dispersed droplets or bubbles, particle-stabilized bicontinuous structures of interpenetrating domains of two different liquids (bijels) have also been proposed as a new class of soft materials for a variety of novel applications.[16]

Despite original advances,[17,18] the understanding of fundamental aspects of nanoparticle adsorption at fluid interfaces has not kept pace with applications.[19] The characterization of nanoparticle assemblies is still an open issue.[20] Measurement of the contact angle of nanoparticles at fluid interfaces and account of the possible effects of line tension on this measurement[21] is also a significant challenge.[6,22−26] As a result, the magnitude of the adsorption energy, which has potentially important consequences for the equilibrium structure of interfacial assemblies and the kinetics of their formation, cannot be accurately predicted from eq 1. Nanoparticle adsorption at fluid interfaces is thermodynamically favored, but the process can be kinetically limited, a situation arising when a significant energy barrier to adsorption exists.[27,28] While it is known that such a barrier is the collective outcome of particle-interface interactions (e.g., electrostatic, van der Waals, hydrophobic) described by Derjaguin−Landau−Verwey−Overbeek (DLVO) theory and its extensions,[3,19,27,28] quantitative links of barrier energy to specific aspects of nanoparticle−interface interactions have not been adequately established.[29−31]

On the basis of thermodynamic considerations, an alternative to eq 1 has been recently proposed:[32]

$$|\Delta E| = \frac{\gamma_0 - \gamma_\infty}{\Theta_\infty} \pi r^2 \quad (2)$$

**Received:** November 11, 2013
**Revised:** December 28, 2013
**Published:** January 7, 2014

   dx.doi.org/10.1021/la404357j | Langmuir 2014, 30, 710−717

where $\gamma_\infty$ and $\Theta_\infty$ are the surface (interfacial) tension and fractional coverage of the interface at steady state, respectively. The latter quantity has been approximated by the greatest possible coverage of the interface, achieved for a hexagonal close packing of nanoparticles ($\Theta_\infty = 0.91$).[32] Equation 2 is an attractive alternative to eq 1 because measurement of the surface (interfacial) tension of a nanoparticle-laden interface is much more straightforward than direct measurement of the contact angle of adsorbed nanoparticles. A number of recent studies have reported the steady state interfacial tension of nanoparticle-laden fluid interfaces.[29−35] Using data from these studies, $|\Delta E|$ computed from eq 2 is plotted in Figure 1.

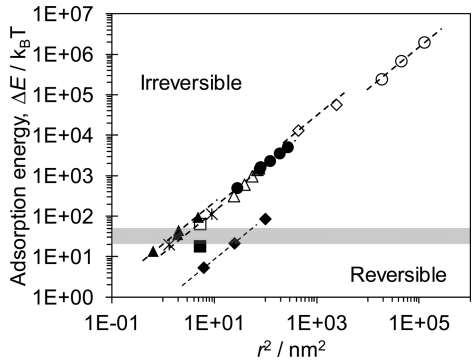


**Figure 1.** Adsorption energy computed from eq 2 for the adsorption of citrate (♦)- and (1-mercaptoundec-11-yl)tetra(ethylene glycol) (TEG) (□)-capped gold nanoparticles at the 2,2,3,3,4,4,5,5-octauoropentyl acrylate (OFPA)−water interface,[32] TEG-capped gold nanoparticles at the 1-fluorohexane (FH)−water interface (■),[32] poly(ethylene glycol) (PEG)-capped iron oxide ($Fe_3O_4$) nanoparticles at the *n*-decane−water interface (●),[35] alkanethiol-capped gold nanoparticles at the hexane−water interface (▲),[30,31] trioctylphosphine oxide (TOPO)-capped cadmium selenide (CdSe) (∗),[29] 1-pentanethiol-capped gold (△),[33] and poly(*N*-isopropylacrylamide) (PNIPAAm)-capped silicon oxide ($SiO_2$) nanoparticles at the toluene−water interface (○),[34] ethyl cellulose (EC) nanoparticles at the air−water interface (◊) (this study). All the dashed lines have a slope equal to unity, as predicted by eq 2.

Evidently, nanoparticle adsorption at fluid interfaces is irreversible in the majority of cases, given that the magnitude of $\Delta E$ delineating reversible and irreversible adsorption lies in the range 20 to 50 $k_BT$. These bounds follow from experimental observations of interfacial tension rebound as the concentration of the bulk colloidal solution surrounding a previously equilibrated drop is reduced[32] and are consistent with the results of computer simulation,[35] which also predicts $\Theta_\infty \cong 0.91$ for irreversible adsorption of nanoparticles.

Dynamic surface (interfacial) tension can be used to probe quantitatively the dynamics of nanoparticle adsorption, provided that a suitable model exists to connect dynamic surface (interfacial) tension to transient coverage of the interface by nanoparticles. To date, dynamic interfacial tension data for nanoparticle colloidal solutions have been analyzed[29−31,36] in terms of the classical model of Ward and Tordai.[37−39] The following asymptotic results[40] have been employed to interpret data from the early ($t \to 0$) and late ($t \to \infty$) stages of nanoparticle adsorption

$$t \to 0: \quad \gamma = \gamma_0 - 2RTC_0\sqrt{\frac{Dt}{\pi}} \tag{3}$$

$$t \to \infty: \quad \gamma = \gamma_\infty + \frac{RT\Gamma_\infty^2}{C_0}\sqrt{\frac{\pi}{4Dt}} \tag{4}$$

where $R$ is the gas constant, $T$ is the temperature, $C_0$ is the molar bulk concentration, $\Gamma_\infty$ is the molar surface concentration at steady state, and $D$ is the nanoparticle diffusion coefficient. Estimates of the latter quantity using eq 3 ($D_{t\to 0}$) and eq 4 ($D_{t\to\infty}$) have yielded $D_{t\to 0} \gg D_{t\to\infty}$, a result attributed to the presence of an energy barrier ($\Delta E_p$) to nanoparticle adsorption at high interfacial coverage,[29,30] which is computed from[38]

$$D_{t\to\infty} = D\exp\left(-\frac{\Delta E_p}{k_BT}\right) \tag{5}$$

where $D$ is the nanoparticle diffusion coefficient predicted by the Stokes−Einstein hydrodynamic theory of diffusion.[41] Whereas $\Delta E$ measures the extent to which nanoparticle adsorption is thermodynamically favored, $\Delta E_p$ determines the extent to which adsorption is kinetically limited. The origin of an energy barrier to nanoparticle adsorption is traced to the interactions between adsorbing colloidal particles and the fluid interface, interactions that vary as the interface transitions from a particle-free state ($t \to 0$) to a particle-covered one ($t \to \infty$).

Understanding the parameters that control the self-assembly, the structure of nanoparticles at the interface, the barrier properties of the assembly, and the rate of particle attachment is the focus of the present investigation. Specifically, we report on the use of dynamic surface tension (DST) measurements to probe the kinetics of irreversible adsorption and self-assembly of hydrophobic, charge-stabilized, ethyl cellulose (EC) nanoparticles[9] at the air−water interface. We demonstrate first a critical flaw with the application of classical eq 3 to DST data under conditions of irreversible adsorption, that is, when $|\Delta E| \gg k_BT$. Linking thermodynamic considerations with the random sequential adsorption (RSA) theory,[42−44] we then put forward and validate a model appropriate for irreversible adsorption of nanoparticles at fluid interfaces. A novel alternative to eq 1 and eq 2 for determining the adsorption energy is obtained. It is further shown that irreversible adsorption kinetics are unequivocally characterized in terms of the adsorption rate constant and the maximum (jamming) coverage, both of which are estimated from DST data for the first time. Strong adsorption of EC nanoparticles at the air−water interface confirms the action of attractive non-DLVO forces and can be explained by the presence of a long-range hydrophobic force.

## EXPERIMENTAL SECTION

**EC Nanoparticle Synthesis.** Minor modifications were made to a reported method[9] of EC nanoparticle synthesis in an aqueous medium. Briefly, a solution (10.7 g $L^{-1}$ or 1.07 g $L^{-1}$) of EC (Sigma-Aldrich, product code: 247499-100G) in HPLC-grade isopropyl alcohol (IPA) (Caledon, product code: 8601-7) was prepared. Following the addition of an equal volume of ultrapure deionized (DI) water (~17 MΩcm), a turbid solution (0.191 mol fraction IPA) is obtained as a result of EC nanoparticle nucleation. Note that IPA−water solutions have an azeotrope at 0.6813 mol fraction of IPA.[45] The solution was enriched in water by boiling under continuous stirring, until the amount of IPA (determined by batch distillation calculations) was less than 0.3 mol%. Colloidal solutions of EC nanoparticles used to measure dynamic surface tension were prepared by


dx.doi.org/10.1021/la404357j | Langmuir 2014, 30, 710−717

dilution of this solution with ultrapure DI water. EC nanoparticles of different radius were prepared (49.5 or 21 nm) depending on the initial concentration of EC in IPA (10.7 g $L^{-1}$ or 1.07 g $L^{-1}$).

**EC Nanoparticle Characterization.** The number-based nanoparticle size distribution and the mean hydrodynamic diameter were determined by dynamic light scattering (Brookhaven Ins. Corp. 90 Plus Particle Size Analyzer) using a refractive index of 1.59.[9] EC nanoparticles were also observed by transmission electron microscopy (TEM). One drop of the colloidal solution (0.1 wt % EC) was trickled on a 200-mesh copper grid and left to dry in air. After complete evaporation of the liquid phase, the copper grid was examined under a Philips CM12 microscope.

**Tensiometry.** We measured the DST of colloidal solutions of EC nanoparticles by axisymmetric drop shape analysis of the profile of pendant drops using equipment and software employed in previous studies[30,31] (VCA 2500 XE, AST Products, Billerica, MA). A preset sample volume (8−12 $\mu$L depending on the EC bulk concentration) was dispensed by a motorized syringe to create a pendant drop from a stainless steel needle. In order to minimize evaporation, the pendant drop was created inside a cuvette covered with Parafilm. A high-speed CCD camera was programmed to capture images of the pendant drop at a specified rate. To facilitate probing of the earlier stages of adsorption (first two minutes from the time the pendant drop is formed), a frame rate of ~10 images/s was used. For capturing later stages of the adsorption (~30 min to ~2.5 h depending on the EC bulk concentration), a frame rate of ~6 images/min was used. The DST of at least three droplets at each concentration was measured in order to assess the reproducibility of experimental data. The surface tension of ultrapure DI water was measured before each experiment with a colloidal solution, and a value of 72.30 ± 0.23 mN $m^{-1}$ was consistently obtained at 295 K in agreement with the literature.[46]

## RESULTS AND DISCUSSION

**Analysis of DST Data.** Aqueous solutions of EC nanoparticles of two different average radii (49.5 or 21 nm) and narrow distribution (Figure S1 in the Supporting Information) were prepared at neutral pH. At this pH, surface-active EC nanoparticles are negatively charged,[9] and their aqueous solutions are stable for months. Figure 2 shows DST data from colloidal solutions of different bulk molar nanoparticle concentrations.

Provided that the bulk concentration is not significantly changed by the attachment of nanoparticles at the interface, the steady state ($t \rightarrow \infty$) surface tension, $\gamma_\infty$, is obtained as the intercept of a plot of $\gamma$ against $(1/t)^{1/2}$, as suggested by eq 4 (see Figure S2 and Figure S3 in the Supporting Information). These values are listed in Table 1. The surface tension plateaus at 38.9 ± 0.6 mN $m^{-1}$, in agreement with a previous study.[9] A battery of control experiments were carried out to confirm that the large reduction in surface tension was due to nanoparticle adsorption at the air−water interface and not due to the adsorption of water-soluble impurities in the starting EC material, as previously suggested.[9] To this end, EC was contacted with ultrapure DI water for at least 3 days, and then the DST of the supernatant was measured (see Figure S4 in the Supporting Information). The quantities of EC and water chosen for this test were such that any surface-active impurities would be present in the supernatant at a concentration

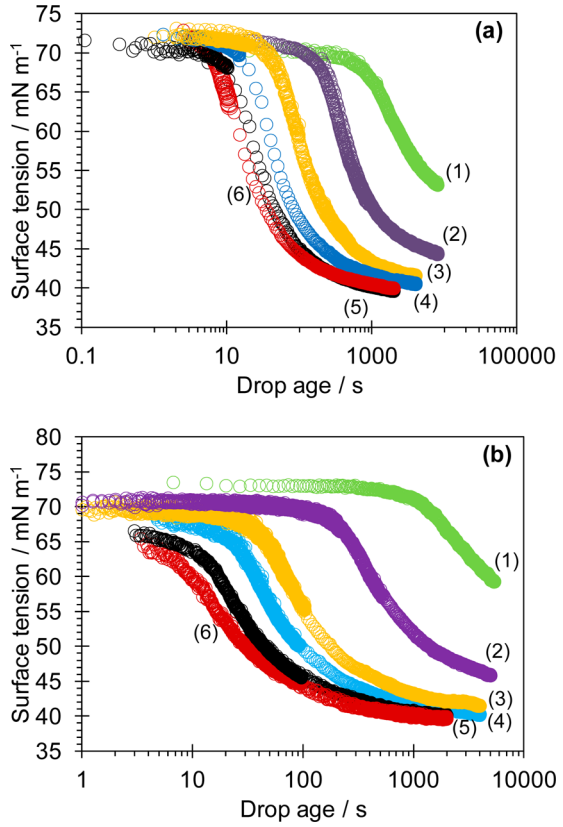


**Figure 2.** Dynamic surface tension (DST) measurements of (a) 89.1 nm (b) 42 nm EC nanoparticles solutions on a log scale plot at concentrations (1) 0.1 g/L, (2) 0.2 g/L, (3) 0.4 g/L, (4) 0.6 g/L, (5) 0.8 g/L, and (6) 1.0 g/L.

equivalent to their concentration in a 2 wt.% EC solution (i.e., at a concentration 20 times greater than their concentration in the most concentrated colloidal solution tested). Measurement of the surface tension of this supernatant yielded a value of ~69 mN $m^{-1}$ after 30 min, which is much greater than the steady state surface tensions realized in the presence of EC nanoparticles. The DST of water−isopropyl alcohol (IPA) mixtures (0.3 mol% IPA or less, corresponding to the concentration of IPA remaining in the various colloidal solutions) in the absence of EC nanoparticles was also measured. The results of these tests (see Figure S5 in the Supporting Information) rule out the presence of small amounts of IPA as the reason for surface tension reduction in colloidal solutions of EC nanoparticles.

In order to analyze the dynamics of the adsorption process, we consider a planar interface and choose a coordinate system with the $x$-axis normal to it and directed toward the solution. A material balance for the adsorbed nanoparticles at the interface ($x = 0$) reads

$$\frac{d\Theta}{dt} = -N_A S j|_{x\rightarrow 0^+} \quad (6)$$

where $\Theta$ is the surface coverage (the fraction of the area of the interface occupied by nanoparticles), $j$ is the molar flux of nanoparticles, $S$ is the area of the interface occupied by a single nanoparticle (i.e., $S = \pi r^2$ for spherical particles), and $N_A$ is Avogadro's number. During the early stages of adsorption ($t \rightarrow 0$), coverage by nanoparticles is low and, in the absence of a


dx.doi.org/10.1021/la404357j | Langmuir 2014, 30, 710−717

Table 1. Steady State Surface Tension ($\gamma_\infty$) and Estimates of Diffusion Coefficient ($D$) Obtained from Analysis of Early-Time DST Data Using Eq 3 and Stokes–Einstein Equation ($D_{S-E}$) for Large (89.1 nm) and Small (42 nm) EC Nanoparticles

| | large EC nanoparticles ($D_{S-E}$ = 4.84 × $10^{-12}$ $m^2$ $s^{-1}$) | | | | small EC nanoparticles ($D_{S-E}$ = 1.03 × $10^{-11}$ $m^2$ $s^{-1}$) | | | |
|---|---|---|---|---|---|---|---|---|
| mass conc. [g $L^{-1}$] | $C \times 10^7$ [mol $m^{-3}$] | $\gamma_\infty$ [mN $m^{-1}$] | $(d\gamma/d\sqrt{t}) \times 10^4$ [N $m^{-1}s^{-0.5}$] | $D \times 10^3$ [$m^2$ $s^{-1}$] | $C \times 10^6$ [mol $m^{-3}$] | $\gamma_\infty$ [mN $m^{-1}$] | $(d\gamma/d\sqrt{t}) \times 10^4$ [N $m^{-1}s^{-0.5}$] | $D \times 10^4$ [$m^2$ $s^{-1}$] |
| 0.1 | 3.93 | 45.00 ± 0.1 | −0.65 ± 0.02 | 3.52 ± 0.2 | 3.75 | 47.38 ± 0.07 | −1.13 ± 0.05 | 1.19 ± 0.1 |
| 0.2 | 7.87 | 41.58 ± 0.05 | −2.03 ± 0.18 | 8.74 ± 1.5 | 7.51 | 42.48 ± 0.1 | −2.23 ± 0.06 | 1.15 ± 0.1 |
| 0.4 | 15.73 | 39.87 ± 0.02 | −4.19 ± 0.21 | 9.25 ± 0.9 | 15.02 | 40.17 ± 0.04 | −8.83 ± 0.10 | 4.51 ± 0.1 |
| 0.6 | 23.60 | 39.34 ± 0.01 | −8.02 ± 0.58 | 15.1 ± 2.2 | 22.53 | 38.95 ± 0.06 | −18.07 ± 0.48 | 8.40 ± 0.4 |
| 0.8 | 31.46 | 38.39 ± 0.01 | −10.44 ± 1.04 | 14.4 ± 2.9 | 30.04 | 38.48 ± 0.05 | −26.82 ± 0.86 | 10.5 ± 0.7 |
| 1.0 | 39.33 | 38.82 ± 0.01 | −13.82 ± 6.64 | 16.1 ± 15.5 | 37.55 | 38.24 ± 0.05 | −40.17 ± 0.44 | 14.9 ± 0.3 |

barrier to adsorption, the interface behaves as a perfect sink. The adsorption flux is then given by Fick's law

$$j|_{x\to 0^+} = -D\frac{\partial C}{\partial x}\bigg|_{x\to 0^+} = -C_0\sqrt{\frac{D}{\pi t}} \tag{7}$$

where $C(x,t)$ is the solution to a simple one-dimensional transient diffusion problem.[41] Substituting eq 7 into eq 6 and integrating gives

$$\Theta = 2\pi r^2 N_A C_0\sqrt{\frac{Dt}{\pi}} \tag{8}$$

Equation 2 may be regarded as a general statement between surface coverage and surface (interfacial) tension at any time

$$\gamma = \gamma_0 - \frac{\Theta}{\pi r^2}|\Delta E| \tag{9}$$

Eliminating $\Theta$ between eq 8 and eq 9 thus gives the novel result

$$\gamma = \gamma_0 - 2N_A|\Delta E|C_0\sqrt{\frac{Dt}{\pi}} \tag{10}$$

It is evident that eq 10 is identical to eq 3 if $|\Delta E| = k_BT$. Both equations predict $\gamma \propto \sqrt{t}$, a well-known trend for diffusion-controlled processes. For $|\Delta E| \gg k_BT$, however, the interpretation of DST data in terms of eq 3 should be expected to grossly overestimate the diffusion coefficient, reliable estimates of which are indeed obtained from the Stokes–Einstein equation ($D = k_BT/6\pi\mu r$) from knowledge of the particle radius and solvent viscosity ($\mu$).[41] The anticipated failure of the Ward and Tordai model to analyze early time DST data for EC nanoparticles is clearly demonstrated in Table 1, which shows estimates of the diffusion coefficient at great odds with theoretical expectations and physical understanding.

The early time DST data (corresponding to $\Theta < 0.3$) may be alternatively analyzed in terms of eq 10 as shown in Figure 3. In this analysis, the diffusion coefficient is appropriately taken equal to the value predicted by the Stokes–Einstein equation for each size of EC nanoparticles. The respective adsorption energy, $\Delta E$, is then estimated from the slope of linear regressions of early time DST data against $\sqrt{t}$ and reported in Table 2. Average values of these estimates only from measurements with colloidal solutions of EC concentration equal to 0.4 g $L^{-1}$ or greater are (5.3 ± 1.0) × $10^4$ $k_BT$ and (0.95 ± 0.02) × $10^4$ $k_BT$ for 89.1 and 42 nm nanoparticles, respectively. Adsorption from solutions containing less than 0.4 g $L^{-1}$ results in significant reduction of the bulk nanoparticle concentration during the course of measurement, consistent with the observation of higher $\gamma_\infty$ values (see Table 1) and in violation of one of the assumptions behind eq 7. The novel

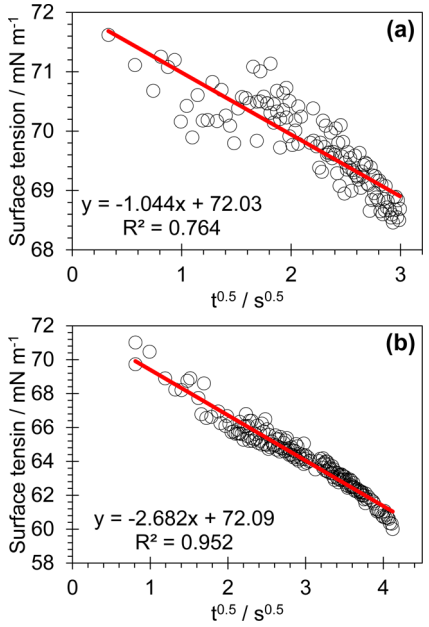


Figure 3. Exemplary plot of early time DST data of (a) 89.1 nm (b) 42 nm EC nanoparticles at a bulk concentration of 0.8 g $L^{-1}$ against $\sqrt{t}$. Solid red lines are linear regressions with parameters indicated in each panel. Results from similar analyses are summarized in Table 1.

estimates of $\Delta E$ based on eq 10 compare very well to the predictions of eq 1, namely, (4.3 ± 0.7) × $10^4$ $k_BT$ and (0.96 ± 0.15) × $10^4$ $k_BT$ for 89.1 and 42 nm EC nanoparticles, respectively, given[9] a contact angle of 68 ± 3°. Predictions of $\Delta E$ from eq 2 assuming $\Theta_{eq}$ = 0.91 are (5.6 ± 0.1) × $10^4$ $k_BT$ and (1.28 ± 0.05) × $10^4$ $k_BT$ for 89.1 and 42 nm EC nanoparticles, respectively, also in good quantitative agreement. We conclude that early time adsorption of EC nanoparticles from an aqueous solution to the air–water interface at neutral pH is quantitatively consistent with the model of barrier-less adsorption described by eq 10.

Unlike eq 2, eq 10 affords an estimate of $\Delta E$ that is independent of assumptions regarding $\Theta_\infty$. The small difference between best estimates of $\Delta E$ from eq 10 and eq 2 supports the conclusion that the maximum (jamming) coverage of the air–water interface by EC nanoparticles (e.g., $\Theta_\infty$ = 0.96 ± 0.18 for 89.1 nm EC nanoparticles) is similar to the coverage corresponding to hexagonal close packing (i.e., $\Theta_{max}$ = 0.91) and significantly greater than what is predicted for localized random sequential adsorption of hard-sphere particles on solid surfaces (i.e., $\Theta_{max}$ = 0.547).[42−44] The difference must be traced to the possibility for lateral rearrangement of nanoparticles adsorbed at a fluid interface, the rearrangement of which is


dx.doi.org/10.1021/la404357j | Langmuir 2014, 30, 710−717

Table 2. Computed Adsorption Energy ($|\Delta E|$) from Eq 10 and Estimates of Adsorption Constant ($k_a$) Obtained from Analysis of Late-Time DST Data Using the Slope of Eq 17 for Large (89.1 nm) and Small (42 nm) EC Nanoparticles

| | large EC nanoparticles | | | | small EC nanoparticles | | | |
|---|---|---|---|---|---|---|---|---|
| mass conc. [g $L^{-1}$] | $\|\Delta E\| \times 10^4$ [$k_BT$] | $[d\gamma/d(1/t)^{1/2}] \times 10^2$ [N $m^{-1}s^{0.5}$] | $K_l \times 10^2$ [−] | $k_a \times 10^6$ [m $s^{-1}$] | $\|\Delta E\| \times 10^4$ [$k_BT$] | $[d\gamma/d(1/t)^{1/2}] \times 10^2$ [N $m^{-1}s^{0.5}$] | $K_l \times 10$ [−] | $k_a \times 10^6$ [m $s^{-1}$] |
| 0.1 | 2.70 ± 0.08 | 71.57 ± 0.78 | 6.73 ± 1.4 | – | 0.34 ± 0.03 | 87.46 ± 0.43 | 3.16 ± 0.15 | – |
| 0.2 | 4.25 ± 0.38 | 25.21 ± 0.31 | 4.74 ± 0.97 | 1.86 ± 0.83 | 0.34 ± 0.01 | 31.75 ± 0.64 | 2.29 ± 0.46 | – |
| 0.4 | 4.37 ± 0.22 | 10.72 ± 0.11 | 4.03 ± 0.82 | 5.55 ± 2.46 | 0.66 ± 0.01 | 17.54 ± 0.14 | 2.53 ± 0.20 | 1.94 ± 0.03 |
| 0.6 | 5.58 ± 0.40 | 7.67 ± 0.04 | 4.32 ± 0.86 | 3.65 ± 1.57 | 0.90 ± 0.02 | 8.94 ± 0.21 | 1.94 ± 0.45 | 2.19 ± 0.10 |
| 0.8 | 5.45 ± 0.54 | 5.76 ± 0.04 | 4.33 ± 0.86 | 5.68 ± 2.47 | 1.01 ± 0.03 | 6.89 ± 0.13 | 1.99 ± 0.37 | 2.07 ± 0.08 |
| 1.0 | 5.77 ± 2.77 | 5.26 ± 0.03 | 4.94 ± 0.98 | 4.42 ± 1.90 | 1.21 ± 0.01 | 6.00 ± 0.11 | 2.16 ± 0.40 | 1.31 ± 0.05 |

controlled by 2-D diffusion within an increasingly dense liquid-like particle layer.[18]

During the later stages of adsorption ($\Theta > 0.75$ in our experiments), as the interface approaches maximum coverage, the presence of already adsorbed particles hinders particle attachment, and the adsorption flux is smaller than predicted by eq 7. In addition to the energy $\phi$ of specific physicochemical interactions (e.g., electrostatic, van der Waals, hydrophobic) between an adsorbing particle and the pristine interface, which are operative during all stages of the adsorption process, there is now an energy $\phi_s$ associated with the interaction between an adsorbing particle and already adsorbed ones. A quantitative account of this interaction, which is essentially steric in nature, is possible in the context of generalized RSA theory, which relates the respective interaction energy to the so-called generalized blocking function $\bar{B}(\Theta)$. This function quantifies the effect of already adsorbed particles on the particle−interface interaction potential and, consequently, on the driving force for adsorption[42,43]

$$\phi_s = -k_BT \ln \bar{B}(\Theta) \tag{11}$$

In the context of generalized RSA,[42,43] the particle flux during the later stages of irreversible adsorption is given by

$$j|_{x\to 0^+} = k_a N_A C_0 \bar{B}(\Theta) \tag{12}$$

where $k_a$ is the adsorption constant, itself a function of diffusion coefficient and specific interaction energy $\phi$, but otherwise unrelated to $\bar{B}(\Theta)$.[42,43] The material balance for adsorbed nanoparticles at the interface is thus written as[42,43]

$$\frac{d\Theta}{dt} = k_a N_A C_0 S \bar{B}(\Theta) \tag{13}$$

Equation 13 may be rewritten in terms of dimensionless parameters ($\bar{k}_a \equiv k_a(L/D)$, $\tau \equiv tD/L^2$, and $L \equiv 1/(N_A C_0 S)$)[42]

$$\frac{d\Theta}{d\tau} = \bar{k}_a \bar{B}(\Theta) \tag{14}$$

For coverage approaching $\Theta_{max}$, a reliable approximation of the blocking function is $\bar{B}(\Theta) \cong 2.32(1 - \Theta/\Theta_{max})^m$, where $m = 3$ for monodisperse spheres.[42,43] This relation shows that steric effects are negligible ($\bar{B}(\Theta) \to 1$) in the early stages of adsorption ($t \to 0$) when only a few particles are present at the interface. Using this approximation into eq 13 and integrating, one gets

$$\Theta = \Theta_{max} - \frac{K_l}{\sqrt{\tau}} \tag{15}$$

where $K_l = \Theta_{max}(\Theta_{max}/4.64k_a)^{1/2}$. Applying the definition of the dimensionless time ($\tau$) results in[42,43]

$$\Theta = \Theta_{max} - \frac{K_l}{\sqrt{(\pi r^2 N_A C_0)^2 Dt}} \tag{16}$$

Finally, elimination of $\Theta$ between eq 16 and eq 9 gives the novel result

$$\gamma = \gamma_\infty + \frac{K_l|\Delta E|}{(\pi r^2)^2 N_A C_0}\sqrt{\frac{1}{Dt}} \tag{17}$$

As shown in eq 17, surface tension varies linearly with $(1/t)^{1/2}$ during the late stages ($t \to \infty$) of an irreversible adsorption process, which is a trend identical to the one predicted by eq 4. Equation 17 is significant because it enables estimation of $K_l$ from the slope $d\gamma/d(1/t)^{1/2}$ given knowledge of the adsorption energy, particle radius, and bulk concentration. In turn, this enables the calculation of the adsorption constant, $k_a$. These calculations are summarized in Table 2.

The maximum value of the interaction energy $\phi$ attributed to specific particle−interface interactions (i.e., the adsorption barrier), $\phi_b$, may be approximately inferred from $k_a$ as follows:[43,47]

$$k_a \cong \frac{D}{r}\sqrt{\frac{\phi_b}{\pi k_BT}}\exp\left(-\frac{\phi_b}{k_BT}\right) \tag{18}$$

One obtains $\phi_b = 3.1\ k_BT$ and $\phi_b = 5.9\ k_BT$ from eq 18 for 89.1 and 42 nm EC nanoparticles, respectively. These estimates are of the order of the mean energy of thermal fluctuations, indicating no significant adsorption barrier arising from the collective action of particle-interface specific physicochemical interactions (electrostatic, van der Waals, hydrophobic, etc.), as also concluded from analysis of the early time DST data. Note that a steric barrier to adsorption is explicitly accounted for in terms of the blocking function. Using eq 11 we estimate the magnitude of a steric barrier as 13 $k_BT$ for $\Theta = 0.9$, valid for any spherical nanoparticle if $\Theta_{max} = 0.91$. It is worth noting that the estimation of an energy barrier to adsorption using a theory that does not discriminate surface blocking effects from particle−interface specific physicochemical interactions, viz. eq 4 and eq 5, yields $\Delta E_p \cong 10\ k_BT$ regardless of EC nanoparticle size (data not shown). Essentially the same result has been obtained for other nanoparticle−fluid systems,[47−50] strongly suggesting that the physical origin of a barrier to nanoparticle adsorption during the later stages is surface blocking. An adsorption barrier of about 10 $k_BT$ is consistent with $D_{t\to\infty}/D = O(10^{-4})$. If adsorption is limited by surface blocking and, therefore, by the rate of lateral rearrangement of adsorbed nanoparticles on the interface, then it is reasonable to expect $D_{t\to\infty}$ to be equal to the 2-D diffusion coefficient ($D_{2D}$) of adsorbed nanoparticles within an increasingly dense liquid-like particle layer. This expectation is not refuted by direct


dx.doi.org/10.1021/la404357j | Langmuir 2014, 30, 710−717

measurement of the 2-D diffusion coefficient in a particle-covered fluid interface,[18] where $D_{2D}/D \propto O(10^{-4})$ is found at high coverage of the interface.

**EC Particle–Particle and Particle–Interface Interactions.** Data and models discussed in the previous section support the conclusion that EC nanoparticles from a colloidal solution at neutral pH adsorb readily onto the air–water interface. The zeta potential of EC nanoparticles at neutral pH is ca. −50 mV,[9] and strong electrostatic repulsion, in the context of classical DLVO theory, explains the stability of their colloidal solutions. Since, however, the zeta potential of the air–water interface at neutral pH is ca. −65 mV,[48] the same theory predicts a very significant barrier to adsorption.[9] Without precluding alternative explanations, we show next that consideration of hydrophobic interactions[27,28] suffices to explain both observations of strong colloidal stability and essentially barrier-less adsorption.

The electrostatic interaction energy ($\phi_{elec}$) between a planar interface and a spherical nanoparticle of radius $r$ separated by a distance $h$ may be computed from[49,50]

$$\phi_{elec} = \pi\varepsilon_0\varepsilon_r r\left\{2\psi_p\psi_c \ln\left[\frac{1+\exp(-\kappa h)}{1-\exp(-\kappa h)}\right] + (\psi_p^2+\psi_c^2)\ln[1-\exp(-2\kappa h)]\right\} \quad (19)$$

where $\varepsilon_0$ (equal to $8.854 \times 10^{-12}$ $C^2$ $J^{-1}$ $m^{-1}$) is the vacuum permittivity, and $\varepsilon_r$ is the relative permittivity of the solvent ($\varepsilon_r$ = 78.5 for water at 25 °C), $\psi_p$ and $\psi_c$ are the surface potential of the particle and the interface, respectively, and $\kappa$ is the inverse Debye length. Surface potentials are approximated here by the respective values of zeta potential and the Debye length ($\kappa^{-1}$) is estimated to be ∼304 nm from solution conductivity measurements (see Supporting Information for details).

The van der Waals interaction energy ($\phi_{vdW}$) between a planar interface and a spherical nanoparticle may be computed from[51]

$$\phi_{vdW} = -\frac{rH_{132}}{6h} \quad (20)$$

where $H_{132}$ is the Hamaker constant for particle (1) interacting with air (2) across water (3). $H_{132}$ is here taken equal to $1 \times 10^{-20}$ J on the basis of published data for cellulosic systems.[52]

The hydrophobic interaction energy may be computed from[27,28]

$$\phi_{hydrophobic} = -\frac{K_{132}r}{h} \quad (21)$$

where $K_{132}$ is the hydrophobic interaction energy constant. The latter may be estimated from the empirical formula $\log K_{132} = a((\cos\theta + \cos\theta_0)/2) + b$, where $\theta$ is the contact angle of a single particle at the interface ($\theta = 68°$ for EC nanoparticles at the air–water interface at pH = 7)[9] and $\theta_0$ is taken equal to 180° for an air–water interface.[27,28] Using the empirical constant values of $a = -7$ and $b = -19.78$, we obtain a value of the hydrophobic constant $K_{132}$ in the lower range of reported values,[27,28] resulting in a conservative account of the hydrophobic interaction energy.

The total interaction between the air–water interface and adsorbing EC nanoparticles at neutral pH is computed as $\phi = \phi_{vdW} + \phi_{elec} + \phi_{hydrophobic}$ and plotted in Figure 4. The calculations indicate a small energy barrier of $\sim 5k_BT$ at a distance of one Debye length from the interface. This energy barrier is similar to $\phi_b$ estimated from DST data. Similar calculations for particle–particle interactions are presented in the Supporting Information. Hydrophobic interactions between two EC nanoparticles are not strong enough to overcome electrostatic repulsion (see Figure S6 in the Supporting Information) and stability of the colloidal solution is again predicted at neutral pH, consistent with experiment.

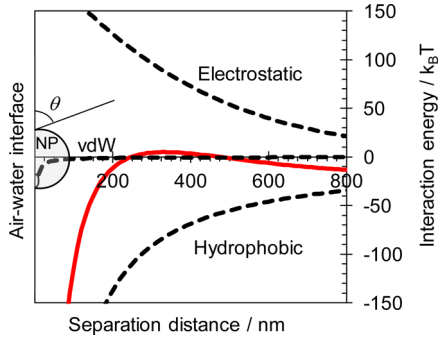


**Figure 4.** Calculated extended DLVO interaction energy profiles between an adsorbing 89.1 EC nanoparticle and air–water interface as a function of separation distance from the interface (drawn to scale). The dashed lines show the profiles of individual interaction energies (i.e., electrostatic, van der Waals, and hydrophobic), whereas the solid red line represents the total interaction energy profile.

## CONCLUSIONS

Dynamic surface tension (DST) can be an extremely informative probe of nanoparticle adsorption at fluid interfaces provided that a competent model is available to connect DST—a readily quantifiable macroscopic property—to the energies of adsorption and particle–interface interaction at different degrees of nanoparticle coverage of the interface. We show that DST models applicable to the adsorption of molecular species do not apply to nanoparticles adsorbing irreversibly. Alternative models inspired by the generalized random sequential adsorption theory are developed and validated for the first time against DST data from a model colloidal system. Ethyl cellulose (EC) nanoparticles, colloidal solutions of which are stabilized by repulsive electrostatic forces at neutral pH, are shown to exhibit barrier-less adsorption at the air–water interface at low surface coverage. This contradicts DLVO predictions, but can be explained by consideration of a hydrophobic force. At high surface coverage, adsorption of EC nanoparticles is limited by a steric energy barrier due to blocking of the interface by already adsorbed nanoparticles. The results of this work advance the potential of DST as a general quantitative probe of parameters controlling the self-assembly, the structure of nanoparticles at the interface, the barrier properties of the assembly, and the rate of particle attachment—parameters that are important for the design and fabrication of novel materials and devices by means of adsorption-driven self-assembly.

## ASSOCIATED CONTENT

### Supporting Information

Dynamic light scattering (DLS) results and transmission electron microscope (TEM) images. Plots of late-time dynamic surface tension (DST) and corresponding analysis. DST of EC–ultrapure DI water supernatant in comparison to the DST of ultrapure DI water. Comparison of DST of solutions with


dx.doi.org/10.1021/la404357j | Langmuir 2014, 30, 710–717

and without nanoparticles. Particle−particle extended DLVO calculations. This material is available free of charge via the Internet at http://pubs.acs.org.

## AUTHOR INFORMATION


### Corresponding Author

*E-mail: mioannid@uwaterloo.ca.


### Notes

The authors declare no competing financial interest.

## ACKNOWLEDGMENTS

The authors acknowledge the financial support of the Natural Sciences and Engineering Research Council of Canada (NSERC) for this work.

## REFERENCES


(1) Pickering, S. U. Emulsions. *J. Chem. Soc. Trans.* **1907**, *91*, 2001−2021.

(2) Böker, A.; He, J.; Emrick, T.; Russell, T. P. Self-assembly of nanoparticles at interfaces. *Soft Matter* **2007**, *3*, 1231−1248.

(3) Binks, B. P. Particles as surfactants − Similarities and differences. *Curr. Opin. Colloid Interface Sci.* **2002**, *7*, 21−41.

(4) Pieranski, P. Two-dimensional interfacial colloidal crystals. *Phys. Rev. Lett.* **1980**, *45*, 569−572.

(5) Binks, B. P.; Lumsdon, S. O. Influence of particle wettability on the type and stability of surfactant-free emulsions. *Langmuir* **2000**, *16*, 8622−8631.

(6) Binks, B. P.; Murakami, R. Phase inversion of particle-stabilized materials from foams to dry water. *Nat. Mater.* **2006**, *5*, 865−869.

(7) Garbin, V.; Crocker, J. C.; Stebe, K. J. Nanoparticles at fluid interface: Exploiting capping ligands to control adsorption, stability and dynamics. *J. Colloid Interface Sci.* **2012**, *387*, 1−11.

(8) Martinez, A. C.; Rio, E.; Delon, G.; Saint-Jalmes, A.; Langevin, D.; Binks, B. P. On the origin of the remarkable stability of aqueous foams stabilised by nanoparticles: Link with microscopic surface properties. *Soft Matter* **2008**, *4*, 1531−1535.

(9) Jin, H.; Zhou, W.; Cao, J.; Stoyanov, S. D.; Blijdenstein, T. B. J.; de Groot, P. W. N.; Arnaudov, L. N.; Pelan, E. G. Super stable foams stabilized by colloidal ethyl cellulose particles. *Soft Matter* **2012**, *8*, 2194−2205.

(10) Binks, B. P.; Rodrigues, J. A. Inversion of emulsions stabilized solely by ionizable nanoparticles. *Angew. Chem., Int. Ed.* **2005**, *44*, 441−444.

(11) Gonzenbach, U. T.; Studart, A. R.; Tervoort, E.; Gauckler, L. J. Ultrastable particle-stabilized foams. *Angew. Chem., Int. Ed.* **2006**, *45*, 3526−3530.

(12) Studart, A. R.; Nelson, A.; Iwanovsky, B.; Kotyrba, M.; Kündig, A. A.; Dalla Torre, F. H.; Gonzenbach, U. T.; Gauckler, L. J.; Löffler, J. F. Metallic foams from nanoparticle-stabilized wet foams and emulsions. *J. Mater. Chem.* **2012**, *22*, 820−823.

(13) Crossley, S.; Faria, J.; Shen, M.; Resasco, D. E. Solid nanoparticles that catalyze biofuel upgrade reactions at the water/oil interface. *Science* **2010**, *327*, 68−72.

(14) Hu, L. F.; Chen, M.; Fang, X.; Wu, L. Oil-water interfacial self-assembly: A novel strategy for nanofilm and nanodevice fabrication. *Chem. Soc. Rev.* **2012**, *41*, 1350−1362.

(15) Cecchini, M.; Turek, V. A.; Paget, J.; Kornyshev, A. A.; Edel, J. B. Self-assembled nanoparticle arrays for multiphase trace analyte detection. *Nat. Mater.* **2013**, *12*, 165−171.

(16) Cates, M. E.; Clegg, P. S. Bijels: A new class of soft materials. *Soft Matter* **2008**, *4*, 2132−2138.

(17) Lin, Y.; Skaff, H.; Dinsmore, A. D.; Russell, T. P. Nanoparticle assembly and transport at liquid−liquid interfaces. *Science* **2003**, *299*, 226−229.

(18) Lin, Y.; Böker, A.; Skaff, H.; Cookson, D.; Dinsmore, A. D.; Emrick, T.; Russell, T. P. Nanoparticle assembly at fluid interfaces: structure and dynamics. *Langmuir* **2005**, *21*, 191−194.

(19) Bresme, F.; Oettel, M. Nanoparticles at fluid interfaces. *J. Phys.: Condens. Matter* **2007**, *19*, 413101−413133.

(20) Turek, V. A.; Cecchini, M. P.; Paget, J.; Kucernak, A. R.; Kornyshev, A. A.; Edel, J. B. Plasmonic ruler at the liquid−liquid interface. *ACS Nano* **2012**, *6*, 7789−7799.

(21) Aveyard, R.; Clint, J. H. Particle wettability and line tension. *Faraday Trans.* **1996**, *92*, 85−89.

(22) Paunov, V. N. Novel method for determining the three-phase contact angle of colloid particles adsorbed at air−water and oil−water interfaces. *Langmuir* **2003**, *19*, 7970−7976.

(23) Arnaudov, L. N.; Cayre, O. J.; Stuart, M. A. C.; Stoyanov, S. D.; Paunov, V. N. Measuring the three-phase contact angle of nanoparticles at fluid interfaces. *Phys. Chem. Chem. Phys.* **2010**, *12*, 328−331.

(24) Mao, Z.; Xu, H.; Wang, D. Molecular mimetic self-assembly of colloidal particles. *Adv. Funct. Mater.* **2010**, *20*, 1053−1074.

(25) Isa, L.; Lucas, F.; Wepf, R.; Reimhult, E. Measuring single-nanoparticle wetting properties by freeze-fracture shadow-casting cryo-scanning electron microscopy. *Nat. Commun.* **2011**, *2*, 438−446.

(26) Kaz, D. M.; McGorty, R.; Mani, M.; Brenner, M. P.; Manoharan, V. N. Physical ageing of the contact line on colloidal particles at liquid interfaces. *Nat. Mater.* **2012**, *11*, 138−142.

(27) Yoon, R. H.; Flinn, D. H.; Rabinovich, Y. I. Hydrophobic interactions between dissimilar surfaces. *J. Colloid Interface Sci.* **1997**, *185*, 363−370.

(28) Xu, L.; Han, G.; Hu, J.; He, Y.; Pan, J.; Li, Y.; Xiang, J. Hydrophobic coating- and surface active solvent-mediated self-assembly of charged gold and silver nanoparticles at water−air and water−oil interfaces. *Phys. Chem. Chem. Phys.* **2009**, *11*, 6490−6497.

(29) Kutuzov, S.; He, J.; Tangirala, R.; Emrick, T.; Russell, T. P.; Böker, A. On the kinetics of nanoparticle self-assembly at liquid/liquid interfaces. *Phys. Chem. Chem. Phys.* **2007**, *9*, 6351−6358.

(30) Ferdous, S.; Ioannidis, M. A.; Henneke, D. E. Adsorption kinetics of alkanethiol-capped gold nanoparticles at the hexane−water interface. *J. Nanopart. Res.* **2011**, *13*, 6579−6589.

(31) Ferdous, S.; Ioannidis, M. A.; Henneke, D. E. Effects of temperature, pH, and ionic strength on the adsorption of nanoparticles at liquid−liquid interfaces. *J. Nanopart. Res.* **2012**, *14*, 850−861.

(32) Du, K.; Glogowski, E.; Emrick, T.; Russell, T. P.; Dinsmore, A. D. Adsorption energy of nano- and microparticles at liquid−liquid interfaces. *Langmuir* **2010**, *26*, 12518−12522.

(33) Rana, S.; Yu, X.; Patra, D.; Moyano, D. F.; Miranda, O. R.; Hussain, I.; Rotello, V. M. Control of surface tension at liquid−liquid interfaces using nanoparticles and nanoparticle−protein complexes. *Langmuir* **2012**, *28*, 2023−2027.

(34) Özlem Nazli, K.; Pester, C. W.; Konradi, A.; Böker, A.; van Rijn, P. Cross-linking density and temperature effects on the self-assembly of $SiO_2$-PNIPAAm core−shell particles at interfaces. *Chem.—Eur. J.* **2013**, *19*, 5586−5594.

(35) Isa, L.; Amstad, E.; Schwenke, K.; Del Gado, E.; Ilg, P.; Kroger, M.; Reimhult, E. Adsorption of core−shell nanoparticles at liquid−liquid interfaces. *Soft Matter* **2011**, *7*, 7663−7675.

(36) Li, Z.; Geisel, K.; Richtering, W.; Ngai, T. Poly(*N*-isopropylacrylamide) microgels at the oil−water interface: Adsorption kinetics. *Soft Matter* **2013**, *9*, 9939−9946.

(37) Ward, A. F. H.; Tordai, L. Time-dependence of boundary tensions of solutions I. The role of diffusion in time-effects. *J. Chem. Phys.* **1946**, *14*, 453−461.

(38) Liggieri, L.; Ravera, F.; Passerone, A. A diffusion-based approach to mixed adsorption kinetics. *Colloids Surf. A* **1996**, *114*, 351−359.

(39) Eastoe, J.; Dalton, J. S. Dynamic surface tension and adsorption mechanisms of surfactants at the air−water interface. *Adv. Colloid Interface Sci.* **2000**, *85*, 103−144.

(40) Fainerman, V. B.; Makievski, A. V.; Miller, R. The analysis of dynamic surface tension of sodium alkyl sulphate solutions, based on asymptotic equations of adsorption kinetic theory. *Colloids Surf. A* **1994**, *87*, 61−75.

(41) Bird, R. B.; Stewart, W. E.; Lightfoot, E. N. *Transport Phenomena*, 1st ed.; John Wiley & Sons, Inc.: New York, 1960.

(42) Adamczyk, Z. Kinetics of diffusion-controlled adsorption of colloid particles and proteins. *J. Colloid Interface Sci.* **2000**, *229*, 477−489.
(43) Adamczyk, Z. Irreversible Adsorption of Particles. In *Adsorption: Theory, Modeling, and Analysis*; Tóth, J., Ed.; Surfactant Science Series; Marcel Dekker Inc.: New York, 2002; Vol. *107*, pp 251−374.
(44) Adamczyk, Z.; Jaszczółt, K.; Michna, A.; Siwek, B.; Szyk-Warszyńska, L.; Zembala, M. Irreversible adsorption of particles on heterogeneous surfaces. *Adv. Colloid Interface Sci.* **2005**, *118*, 25−42.
(45) Ruckenstein, E. Reversible rate of adsorption or coagulation of Brownian particles − Effect of the shape of the interaction potential. *J. Colloid Interface Sci.* **1978**, *66*, 531−543.
(46) Graciaa, A.; Morel, G.; Saulner, P.; Lachaise, J.; Schechter, R. S. The $\zeta$-potential of gas bubbles. *J. Colloid Interface Sci.* **1995**, *172*, 131−136.
(47) Hogg, R.; Healy, T. W.; Fuerstenau, D. W. Mutual coagulation of colloidal dispersions. *Trans. Faraday Soc.* **1966**, *62*, 1638−1651.
(48) Liu, Y.; Zhang, C.; Hilpert, M.; Kuhlenschmidt, M. S.; Kuhlenschmidt, T. B.; Nguyen, T. H. Transport of cryptosporidium parvum oocysts in a silicon micromodel. *Environ. Sci. Technol.* **2012**, *46*, 1471−1479.
(49) Evans, D. F.; Wennerström, H. *The Colloidal Domain: Where Physics, Chemistry, Biology, and Technology Meet*, 2nd ed.; Wiley-VCH; New York, 1999.
(50) Bergström, L.; Stemme, S.; Dahlfors, T.; Arwin, H.; Ödberg, L. Spectroscopic ellipsometry characterisation and estimation of the Hamaker constant of cellulose. *Cellulose* **1999**, *6*, 1−13.
(51) Brunjes, A. S.; Bogart, M. J. P. Vapor−liquid equilibria for commercially important systems of organic solvents: The binary systems ethanol−*n*-butanol, acetone−water and isopropanol−water. *Ind. Eng. Chem.* **1943**, *35*, 255−260.
(52) Vargaftik, N. B.; Volkov, B. N.; Voljak, L. D. International tables of the surface tension of water. *J. Phys. Chem. Ref. Data* **1983**, *12*, 817−820.